Emissivity measurement of the ITER-like plasma facing components of the WEST phase 2: Pre-exposure measurements and first WEST exposure

J. Gaspar, F. Rigollet, N. Ehret, Y. Anquetin, E. Bernard, Y. Corre, M. Diez, M. Firdaouss, M. Houry, T. Loarer, et al.

Emissivity measurement of the ITER-like plasma facing components of the WEST phase 2: pre-exposure measurements and first WEST exposure

J. Gaspar[1], F. Rigollet[1], N. Ehret[1], Y. Anquetin[1], E. Bernard[2], Y. Corre[2], M. Diez[2], M. Firdaouss[2], M. Houry[2], T. Loarer[2], C. Martin[3], M. Missirlian[2], P. Moreau[2], C. Pocheau[2], P. Reihlac[2], M. Richou[2], E. Tsitrone[2] and the WEST team[4]

[1] *Aix Marseille Univ, CNRS, IUSTI, Marseille, France*

[2] *CEA Cadarache, IRFM, F-13108 St Paul lez Durance, France*

[3] *Aix Marseille Univ, CNRS, PIIM, Marseille, France*

[4] *See http://west.cea.fr/WESTteam*

Corresponding author email address: jonathan.gaspar@univ-amu.fr

Abstract. This paper summarizes the emissivity measurements performed on the shaped ITER-like plasma facing units (PFU) of the WEST lower divertor installed for the second phase of WEST. Laboratory measurements before their installation in WEST, as well as measurement of one ITER-like PFU after exposure to an experimental campaign are shown. The measurements of 24 standard ITER-like PFU show the emissivity variability from 0.07 to 0.2 even for a serial production. Measurements performed after high heat flux tests (10 MW/m² cycles) on two different facilities show the emissivity modification induced by this heat load capability test with mainly a decrease of the emissivity in the heat load area. Finally, the exposed ITER-like PFU exhibit a complex pattern with strong emissivity variation from 0.05 in the net erosion area at the strike point locations up to 0.85 in the deposition area close to the strike point location.

1. Introduction

Infrared (IR) thermography is widely used in fusion research to study the heat load distribution on the plasma facing units (PFU) [1-3] as well as ensuring their protections [4-7]. To these ends, assessing the emissivity of tungsten (W) components, as used for the ITER divertor [8], is necessary to derive accurate surface temperature from radiation measured by infrared systems [9]. The W emissivity is low and dependent on various parameters as wavelength, temperature, and surface state such as its composition (oxidation, impurities) and its structure (roughness, cracks, deposited layers) [10]. During plasma operation, the PFU surface state evolves with time because of the plasma wall interaction processes which are likely different from pulse to pulse. Consequently, it strongly affects the emissivity values and distributions observed during the first phase of WEST [11].

This paper presents the emissivity measurements performed for the preparation of the second phase of WEST. For this phase the whole lower divertor is equipped with shaped ITER-like PFU with 1° toroidal bevel as expected for ITER [12]. The first part of the paper describes the lower divertor, the ITER-like PFU geometry and the testbed used to perform emissivity measurement. Then emissivity measurements performed on ITER-like PFU before their installation are shown, with standard PFU but also for PFU before and after high heat load tests. Finally, emissivity measurement of one exposed ITER-like PFU of the phase 2 is shown and compared to the experimental campaign exposure.

2. WEST lower divertor phase 2

The phase 1 of operation of WEST extending from 2017 to 2020 is composed by five experimental campaigns named from C1 to C5 [13]. During this phase, the lower divertor was composed of a mix of actively cooled unshaped ITER-like and inertially cooled W-coated graphite PFUs. For the second phase of operation starting in 2022, the lower divertor is fully equipped with shaped ITER-like PFUs with ITER relevant shaping, allowing plasma operation with long and high-energy pulses [14]. As the lower

divertor is composed by 12 independent toroidal sectors equipped by 38 plasma facing units (PFUs) each, a total of 456 ITER-like PFUs have been manufactured and delivered by the Chinese company AT&M to cover the full divertor ring [12]. The 456 PFUs were delivered within 9 'delivery batches' to CEA, acceptance tests have been performed all along the manufacturing period [15]. Among the 456 PFUs, 59 PFUs are manufactured with special features as for dedicated diagnostics [16].

Each ITER-like PFU (figure 1) is made of 35 W monoblocks (MB) assembled on a CuCrZr heat sink tube via a copper interlayer ring, using hot isostatic pressing as assembly process. The total length of a PFU is 437 mm with MB dimensions of (26.3 to 31.8)mm×12mm×26mm (toroidal×poloidal×height) and 0.5mm of inter-MB gap. Material specifications are coming from ITER specifications [8] giving criteria and various material properties, such as content, density, mechanical properties and grain size. On WEST, divertor is just below the magnetic X-point, with the two strike points impacting the same PFU. Therefore, the shaping has different orientation along the PFU in the inner strike point (ISP) region (MB #1 to #19) and outer strike point (OSP) region (MB #24 to #35). A transition area (MB #20 to #23, see figure 1) without shaping, to accommodate the private flux area, complete the PFU. The shaping is a 1° bevel, around 0.5mm height, corresponding to the baseline ITER shaping [17]. This 'fish-scale' shaping aims at protecting leading edges (edge on the PFU side facing the incident field lines) in case of misalignment. In addition, the leading edges have a 1×1 mm chamfer, to avoid sharp edges on the leading edge in case of high misalignment [18]. This bevel is made during the last manufacturing process using electro discharge, grinding and milling [12].

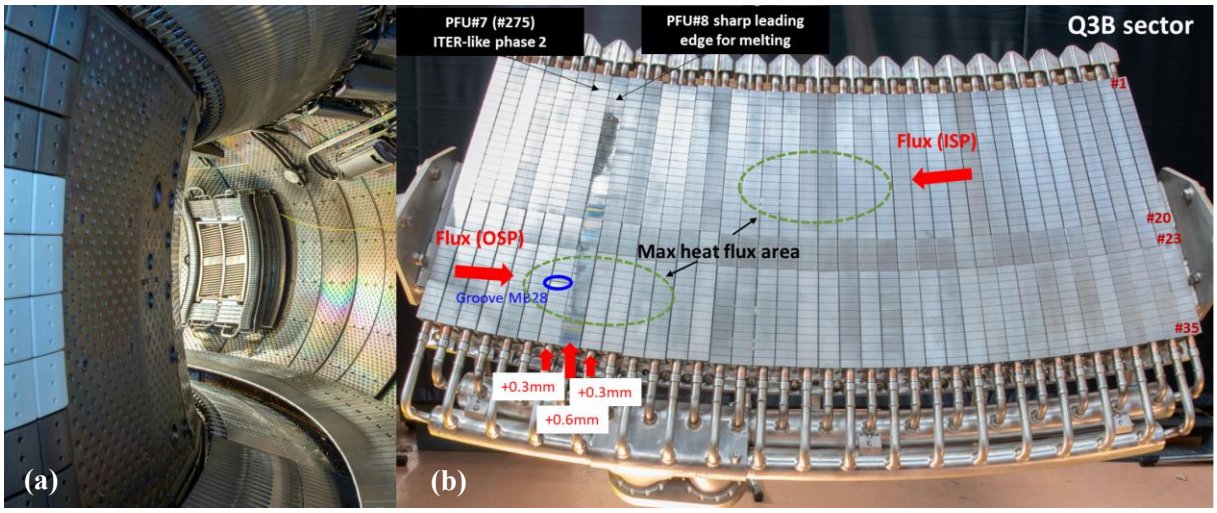

Figure 1. (a) Picture of WEST before the C5 experimental campaign. (b) Picture of the Q3B sector equipped with 35 bevelled ITER-like PFU and one unshaped ITER-like PFU (PFU#8). Vertical misalignments are indicated (red) as well as plasma direction (black) and maximum heat load location due to the ripple modulation (green dotted circle)

3. The ITER-like PFU emissivity testbed

A dedicated testbed has been developed to measure the emissivity map of the full PFUs (see figure 2) based on the double heating method [19]. The emissivity map is calculated by:

$$\varepsilon = \frac{(L_{m1} - L_{m2})}{(L_{BB1} - L_{BB2})} \quad (1)$$

with

$$L_{m1} = \varepsilon L_{BB1} + L_{r1} \quad (2)$$

$$L_{m2} = \varepsilon L_{BB2} + L_{r2} \quad (3)$$

Where ε is the emissivity (supposed unchanged or low variation at the two temperatures), L_{m1} and L_{m2} are the measured radiances at the PFU temperatures T_1 and T_2, L_{BB1} and L_{BB2} are the blackbody radiances computed with the temperatures T_1 and T_2 given by TCs in the water loop. As we control the testbed environments, we can consider here that the reflected radiance measured at each temperature is equal (L_{r1}=L_{r2}) simplifying the emissivity calculation contrary to the tokamak case where the reflected radiance behavior must be assessed by photonic calculation [19].

Two thermostatic baths are used to heat up the PFU at the two different temperatures using the CuCrZr tube. The PFUs are heated at T_1=30°C and T_2=70°C, at each temperature the PFUs are measured by an IR camera in the wavelength range from 3 to 5 µm, to optimize the signal noise ratio at this temperature level. The frame size is of 640×512 pixels, a 25 mm lens is used to get the full PFUs with a projected pixel about 0.7mm/pixel. For some ITER-like PFUs a 50 mm lens with an extension ring is used to have a field of view of about 4 monoblocks of the ITER-like PFU with a projected pixel of about 0.08mm/pixel close to the very high-resolution IR view that monitors the ITER-like PFU of the Q3B sector [20]. The uncertainty on the measured emissivities is about 4% and has been evaluated with Monte Carlo calculation considering errors on the PFU temperature of 1 °C and uncertainties on the IR calibration optimized for these measurements. This uncertainty will be displayed on some figures and removed for other for clarity. In any case, the uncertainty on the measured emissivity remains much lower than the spatial distribution observed even for unexposed PFU.

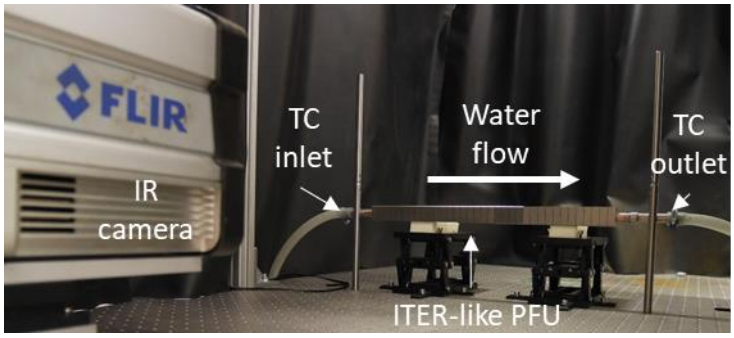

Figure 2. Picture of the ITER-like PFU emissivity testbed.

4. Emissivity measurement performed on the ITER-like PFU before WEST exposure

4.1. Emissivity distribution of the standard ITER-like PFU

Further to the acceptance tests [15] and before their installation in WEST, emissivity measurements have been performed on 24 ITER-like PFUs (about 5% of the whole divertor). Figure 3 shows (a) the emissivity maps of 7 ITER like-PFUs representative of the whole set of PFUs and (b) the average emissivity for each MB (color scale) of the whole set (24 PFUs) and the average emissivity for each MB (black). Three different area appear corresponding to the different shaping manufactured on the PFU with the 1° bevel on ISP region (MB #1 to #19) as well as on the OSP region (MB #24 to #35) and the transition area with flat MB (MB #20 to #23). The bevelled regions exhibit equivalent and higher emissivity values (scattered from ≈0.07 to ≈0.2) than the flat region where emissivity values are scattered from ≈0.06 to ≈0.12. Despite the factor 3 in the bevelled region each MB exhibits relatively uniform emissivity in comparison to the amplitude variation over the whole set. The higher emissivity in the bevelled regions can be explained by the manufacturing step (the whole steps can be found in [12]). Indeed, the 1° bevel is the final manufacturing step with electrical discharge machining, grinding and

milling. This step modifies the MB roughness and the surface pollution. Fig 3 c) shows the average emissivity for each MB versus the roughness measured with confocal microscopy [21]. The circles with the same color scale as fig 2 b) shows the emissivity increase with the roughness of the bevelled MB. The roughness goes from 0.3µm to 1.45µm corresponding to emissivity from 0.07 to 0.2, respectively. For the flat MB (black triangle) the roughness dispersion is lower from 0.3 to 0.8µm (emissivity respectively between 0.07 and 0.12). As expected, the roughness is well correlated to the emissivity for unexposed PFU with the same type of roughness (here machining) and equivalent surface pollution [10]. The 24 ITER-like PFUs come from different batches, no correlation has been found between the batch and the measured emissivity or roughness showing the variability of the final emissivity for a serial production of ITER-like PFU.

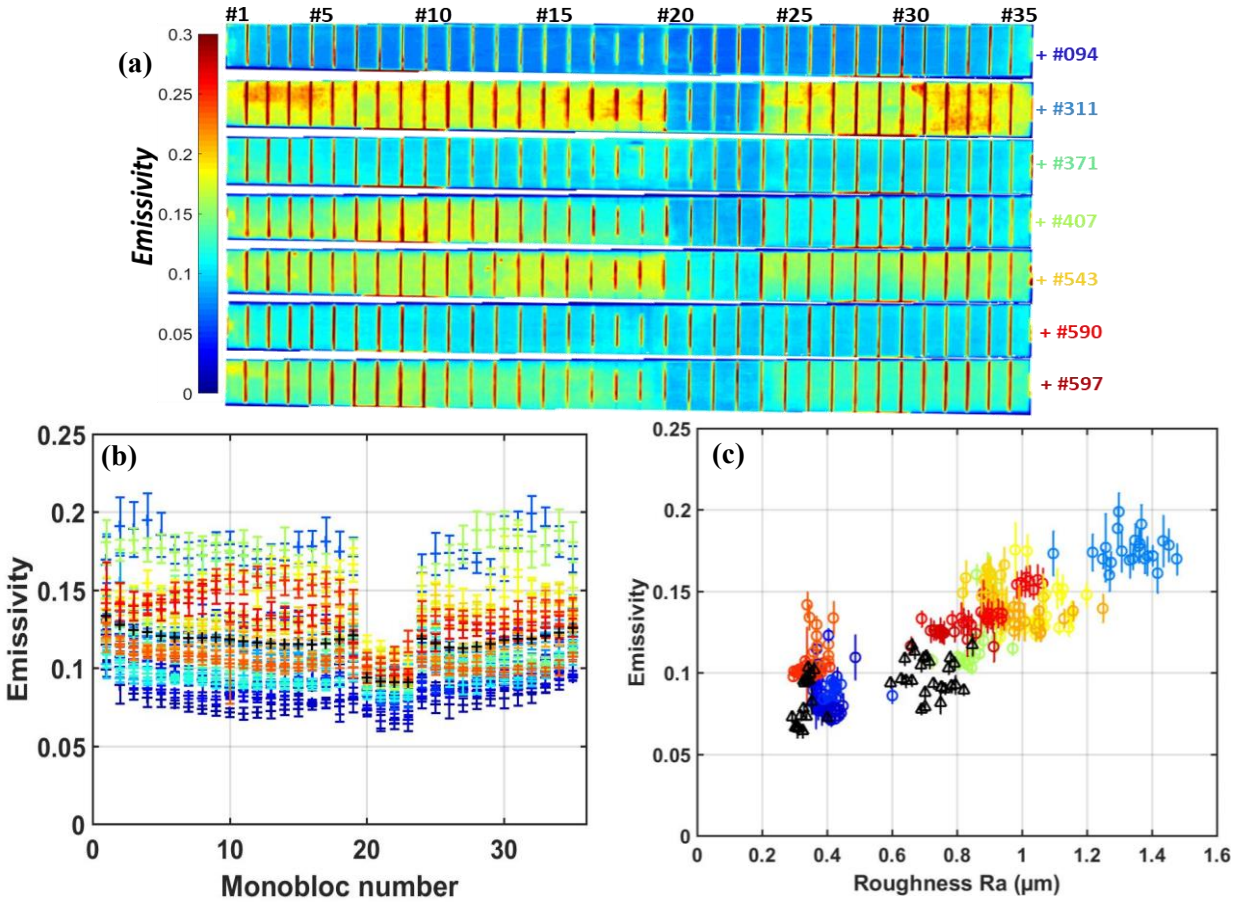

Figure 3. (a) Emissivity map of 7 ITER-like PFUs of the WEST phase 2 before exposure in WEST. (b) Average emissivity for each MB for 24 ITER-like PFUs (color scale) and PFUs average (black) of the WEST phase 2 before installation. (c) Average emissivity for each beveled MB for 12 ITER-like PFUs (circle with same color scale as fig b)) versus the MB roughness and flat MB (black triangle). The error bar corresponds to the uncertainty of the measurement (due to TC and IR uncertainties) and the spatial distribution over the MB.

4.2. Emissivity evolution due to the high heat flux qualification tests

After their reception, acceptance tests were performed at CEA [15]. Some tests are performed for all PFU as the dimensional and visual tests ensuring the feasibility to attach mechanically the PFUS on sectors. Since the PFUs have to sustain heat load of 10MW/m², heat exhaust tests are performed using

infrared thermography [22] and High Heat Flux (HHF) facilities as GLADIS with ion beam [23] and HADES with electron beam. A total of 23 PFUs have been tested in HHF facilities. The HHF test consists of heat load cycling with an amplitude of 10MW/m² and cycle with 10s of heating ensuring to reach the steady state behavior of the PFUs. Different locations are tested along the PFU with different number of cycles for the two HHF facilities and, for each location, 5 MB are exposed to the 10MW/m² heat load.

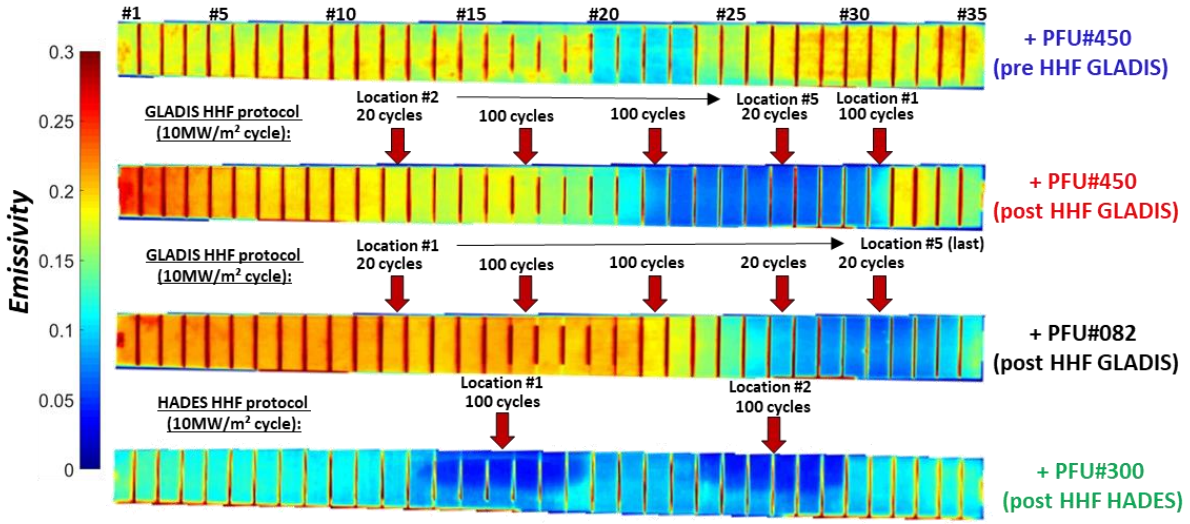

Figure 4. Emissivity map before and after high heat flux (HHF) tests for the PFU #450 and after HHF for PFU#082 performed at GLADIS and PFU#300 after HHF performed at HADES. Heat load location and order are indicated by red arrows. At each location about 5MB are exposed.

Figure 4 shows the emissivity measurements for 3 PFUs after their HHF test, the HHF protocols are also illustrated above each PFU. For the PFU#450 the emissivity measurement has been also performed before HHF test. Figure 5 shows the average emissivity for each MB for the 3 PFUs and the purple area corresponds to the emissivity dispersion observed for the 24 measured PFUs shown in figure 3. The comparison of the pre and post HHF measurements of the PFU#450 clearly shows the emissivity modification of the PFU due to the heat load exposure in GLADIS. The emissivity distribution of the standard phase 2 PFU shown in the figure 3, with low emissivity on the flat area and high emissivity on the beveled area, has been changed with a low emissivity of about 0.064 ± 0.004 for the MB#23 to 30 and high emissivity on the rest of the PFU up to 0.248 ± 0.01 for the MB#1 which was initially at 0.181 ± 0.014. For the MB#27 the emissivity has been reduced from 0.179 ± 0.012 down to 0.063 ± 0.004. This new emissivity distribution is due to the sequential ordering in time of the heat load location. If the sequence of heat loading would be reverted (starting from location #5 and ending to location #1) the low emissivity area would be at the location #1. The emissivity map of the PFU#082 shows clearly that the low emissivity area is always at the last location of the heat load and not in the area with the highest number of cycles. This shows that the emissivity varies rapidly during the first cycles as already observed in such facility [24]. One can note an increase of the emissivity for the first MBs from #1 to #11 with higher emissivity in comparison to the pre HHF measurement and also high emissivity in the first loaded areas showing a possible pollution of the surface during the cycles. For the PFU#300 tested in HADES the emissivity map is different. The emissivity is lowest in the loaded area down to 0.054 ± 0.016 with non-uniform emissivity on the MB. Contrary to the other PFUs, the loaded areas exhibit equivalent emissivity pattern and the rest of the PFU is still in the range of the standard phase 2 PFU showing low pollution of the surface. For the next HHF tests systematic emissivity and confocal measurements will be performed before and after HHF tests to study these emissivity modifications.

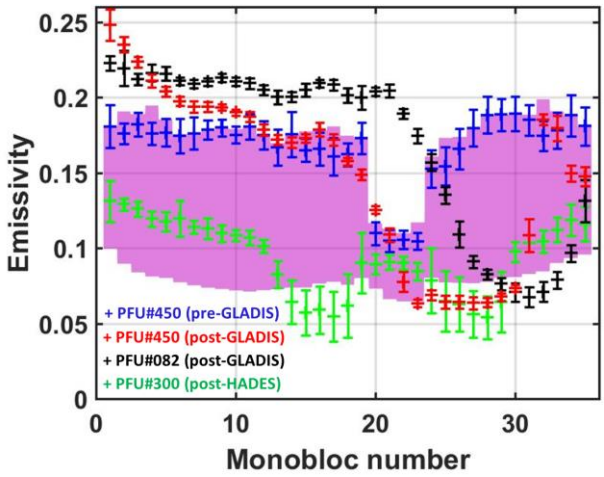

Figure 5. Average emissivity for each monobloc with distribution interval before and after high heat flux (HHF) test for the PFU #450 (blue and red) and after HHF for PFU#082 (black) performed at GLADIS and PFU#300 (green) after HHF performed at HADES. The purple area corresponds to the emissivity dispersion observed for the 24 measured PFUs shown in figure 3b.

5. Emissivity evolution after C5 campaign for PFU phase 2

During the shutdown before C5, last campaign of the WEST phase 1, the W-coated PFUs and the unshaped ITER-like PFUs of two sectors, have been replaced by ITER-like PFUs with toroidal bevel of 1° as expected in ITER. From the 76 PFUs only one unshaped ITER-like PFU has been kept for C5 and installed at the location #8, where heat load is maximum due to the ripple modulation, in order to perform melting experiment on the MB#28 [25]. To achieve melting, a 2mm deep groove was machined in the upstream bevelled ITER-like PFU#7 (see figure 1b). After C5 the standard phase 2 PFU#7 with the groove has been removed from the machine and emissivity measurement has been performed, giving the opportunity to investigate the variation of the emissivity of a standard phase 2 PFU after one experimental campaign.

Figure 6 shows the emissivity of the phase 2 ITER-like PFU exposed only to the C5 campaign. During this campaign a duration of about one hour of diverted deuterium plasma has been performed with a cumulated energy to the divertor of 1.78 GJ. Despite the relatively low level of exposure (three times lower than the C4 exposure) the PFU emissivity is clearly outside the measured range of unexposed phase 2 ITER-like PFU (green area in the figure 6). The emissivity exhibits strong spatial variations coherent with previous observations performed on the phase 1 PFUs [11]. In the strike point areas, a clear decrease of the emissivity is observed down to 0.05 on the inner side (MB# 14 to #16) and outer side (mainly MB#24 to #26) coherent with net erosion area [26]. Few MB away to these areas, high emissivity is found on both side with emissivity up to 0.85 and large variations over a single MB as for the MB#11 with emissivity from 0.4 to 0.85. Three areas remain in the unexposed emissivity range, the first one is for the first MB in the inner side of the PFU far away to the inner strike point area that could be due the moderate duration of the campaign and the low number of boronization performed with only two boronizations for C5 contrary to the thirteen boronizations performed during C4 [13]. The second area is in the private flux region area also corresponding to the flat MB#20 to #23. The last area is on the last MB on the outer side under the baffle which implies magnetically shadowed area from the MB#32 where the emissivity is the highest on the outer side.

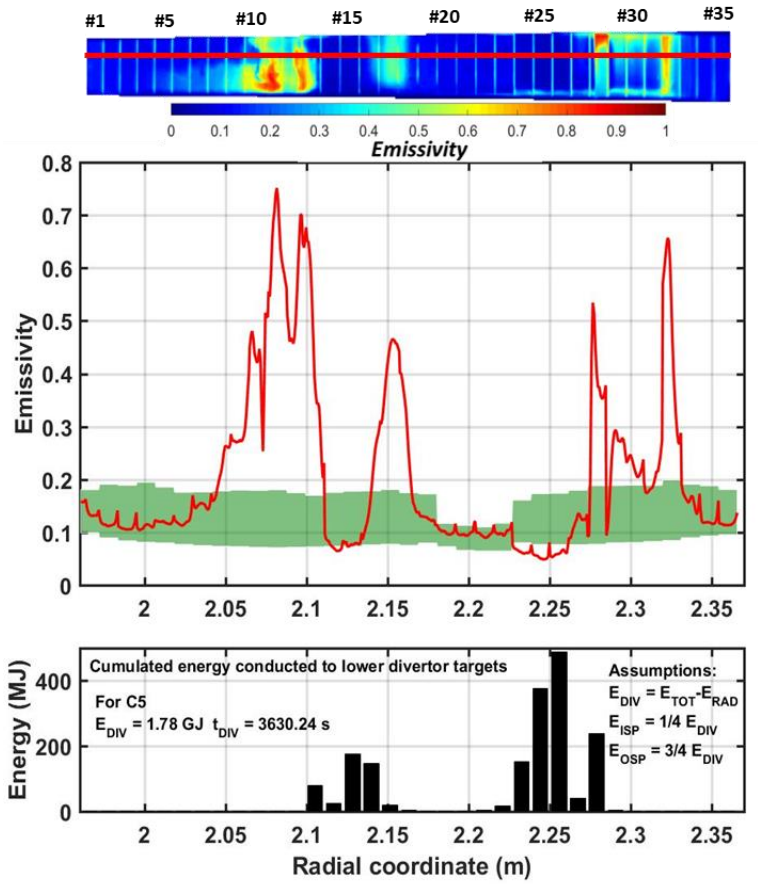

Figure 6. (Top) Emissivity map of the ITER-like phase 2 PFU #7 from the sector Q3B after C5. (Middle) Emissivity distribution along the lower divertor in red and green area corresponds to the emissivity dispersion observed for the 24 measured PFUs shown in figure 3. (Bottom) Conducted energy during C5 to the lower divertor at the strike point location with asymmetry of 1/4 ISP and 3/4 OSP as observed in [27] and no consideration of decay length (λ_q).

Figure 7 shows the emissivity of the top and lateral surfaces of the PFU#7 after C5 for the full PFU and zoom in at both strike point areas. On the PFU sides, on both leading and trailing edges, the measurement shows low and high emissivity on the wetted and shadowed areas respectively. The high emissivity area suggests impurity deposition in the inter-PFU gap of 0.5 mm. This impurity deposition occurs from the MB#10 to #18 on the high field side and from MB#23 to #31 on the low field side corresponding to a poloidal extension higher than the strike point locations. Figure 8 shows the emissivity along the curvilinear abscissa for the MB at both strike point locations with identification of the leading and trailing edge. The measurement exhibits high emissivity ~0.6 up to 2 mm below the top surface for both trailing edges and up to 0.4 for the leading edges. For the leading-edge high emissivity of 0.4 appears also on the first 2mm of the top surface which is also magnetically shadowed due to the MB beveling. On the lateral sides below the 2mm depth, the emissivity decreases down to ~0.1 which indicates the limit of the plasma impact during C5. The MB#28 (magenta in fig 8 b)) exhibits high emissivity in the groove up to 0.85 close to the trailing-edge before the next PFU where the melting experiment occurs and could have induced important impurity production and local redeposition in the groove.

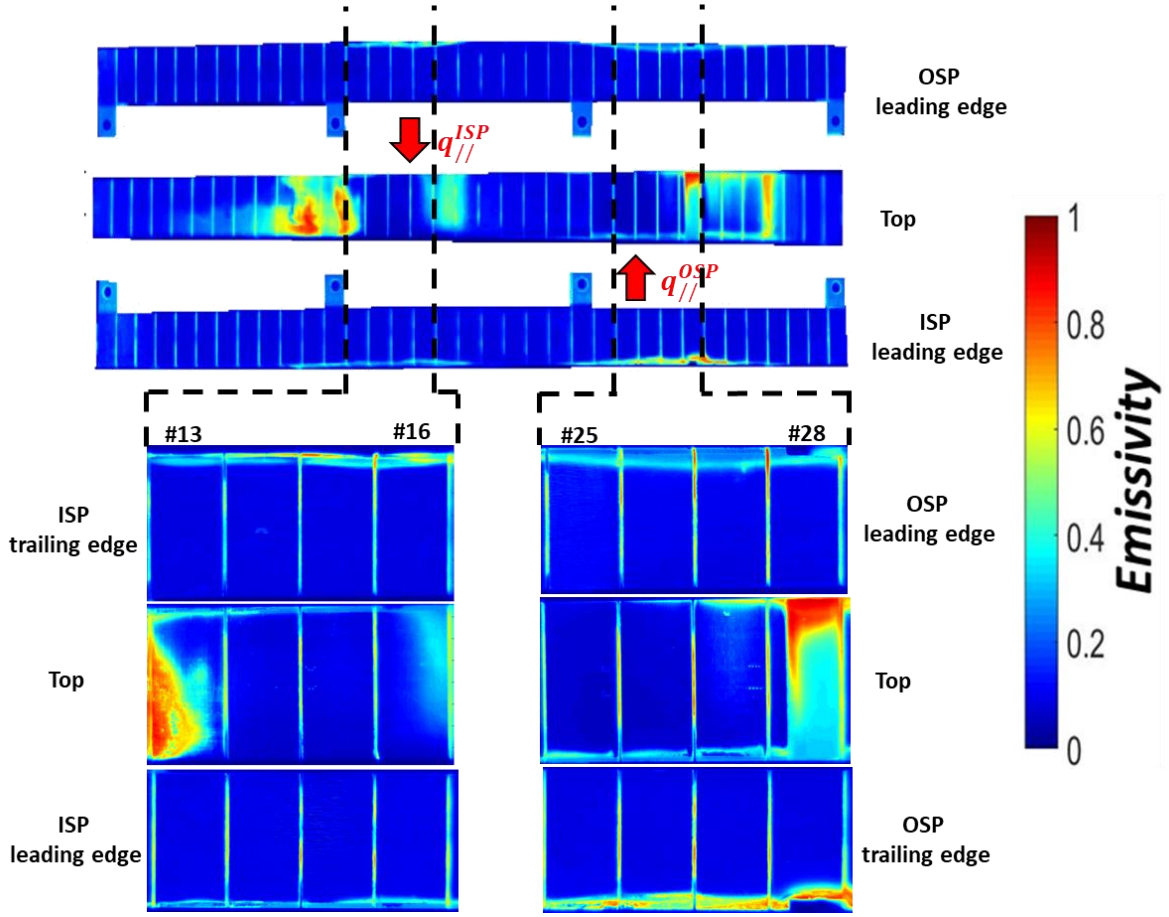

Figure 7. Emissivity map of the PFU #7 after C5. (top) Full PFU with top and lateral sides with 25 mm lens (0.7mm/pixel, full length analyzed of 437mm). (bottom) Zoom in for 4 MBs at the inner (left) and outer (right) strike point locations with 50 mm lens (0.08mm/pixel, full length analyzed about 50mm).

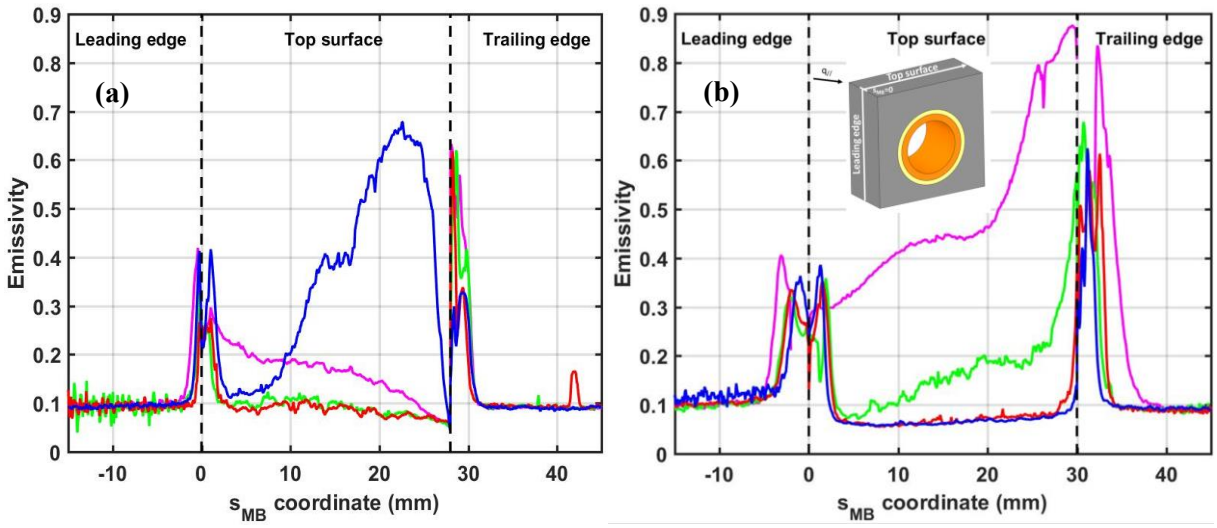

Figure 8. Emissivity of PFU #7 after C5 measured in the MB center along the curvilinear abscissa s_{MB} with s_{MB} =0 mm at the junction between the leading-edge and the top surface. (a) Inner strike point MB (blue) #13, (red) #14, (green) #15 and (magenta) #16. (b) Outer strike point MB (blue) #25, (red) #26, (green) #27 and (magenta) #28 inside the groove.

6. Conclusion

A total of 456 ITER-like PFUs, with 1° toroidal bevel as expected for ITER, have been installed in the WEST lower divertor for the second phase of WEST. Emissivity measurements have been performed on 24 ITER-like PFU before their installation. Three different areas appear corresponding to the different shaping manufactured on the PFU with the 1° toroidal bevel on ISP region as well as on the OSP region and the transition area with flat MB. The bevelled regions exhibit equivalent and higher emissivity values (scattered from ≈0.07 to ≈0.2) than the flat region where emissivity values are scattered from ≈0.06 to ≈0.12. The higher emissivity in the bevelled regions is due to the final machining with electrical discharge machining, grinding and milling. This step increases the MB roughness as well as the surface pollution inducing higher emissivity. No correlation has been found between the manufactured batches and the PFU emissivity showing a variability of a factor 3 on the emissivity even for a serial production of ITER-like PFU.

Emissivity measurements have been also performed on ITER-like PFU after HHF tests at GLADIS and HADES. These measurements have shown a clear modification of the PFU emissivity depending on the HHF facility and the HHF protocol. A decrease of about a factor 3 has been measured after HHF test in the last loaded area.

During the last campaign of the WEST phase 1, called C5, 75 phase 2 ITER-like PFUs have been already installed in the lower divertor. After the campaign, one PFU has been removed and emissivity measurement has shown important modification of the emissivity as expected. Despite the relatively low level of exposure (three times lower than the C4 exposure) the PFU emissivity is clearly outside the measured range of unexposed PFUs. In the strike point areas, a clear decrease of the emissivity is observed down to 0.05 on the inner and outer strike point areas coherent with net erosion area. Few MB away, high emissivity is found on both side with emissivity up to 0.85 (factor of 17 variations of the emissivity along the PFU, between erosion and redeposition areas). On the most loaded area, in the vicinity of the strike point areas, variation of 50% has been found in few cm distance. In this area where measurement is very important, this spatial distribution can induce an error ranging from 20 to 70% on the surface heating assessed by the IR measurement during the pulse and close to 40% on the heat flux width at the target obtained with IR measurements. The PFU sides have been also investigated, showing high emissivity ~0.6 for both trailing-edges and up to 0.4 for the leading-edges up to 2 mm below the top surface while the inter-PFU gap is 0.5mm.

Acknowledgments
This work has been carried out within the framework of the EUROfusion Consortium, funded by the European Union via the Euratom Research and Training Programme (Grant Agreement No 101052200 — EUROfusion). Views and opinions expressed are however those of the author(s) only and do not necessarily reflect those of the European Union or the European Commission. Neither the European Union nor the European Commission can be held responsible for them.

References
[1] A. Grosjean et al., “First analysis of the misaligned leading edges of ITER-like plasma facing units using a very high resolution infrared camera in WEST”, Nuclear Fusion 60 (2020) 106020.

https://doi.org/10.1088/1741-4326/ab9fa6
[2] B. Sieglin et al., “Power load studies in JET and ASDEX-Upgrade with full-W divertors”, Plasma Phys. Control. Fusion 55 (2013) 124039. https://doi.org/10.1088/0741-3335/55/12/124039
[3] B. Sieglin et al., “Real-Time Infrared Thermography at ASDEX Upgrade”, Fusion Science and Technology 69 (2016) 580–585. https://doi.org/10.13182/FST15-183
[4] X. Courtois et al., “Full coverage infrared thermography diagnostic for WEST machine protection”, Fusion Engineering and Design 146 (2019) 2015–2020. https://doi.org/10.1016/j.fusengdes.2019.03.090
[5] I. Balboa et al., “Upgrade of the infrared camera diagnostics for the JET ITER-like wall divertor”, Review of Scientific Instruments, 83 (2012) 10D530. https://doi.org/10.1063/1.4740523
[6] G. Arnoux et al., “A protection system for the JET ITER-like wall based on imaging diagnostics”, review of scientific instruments, 83 (2012) 10D727. https://doi.org/10.1063/1.4738742
[7] M. Jakubowski et al., “Infrared imaging systems for wall protection in the W7-X stellarator”, Review of Scientific Instruments, 89 (2018) 10E116. https://doi.org/10.1063/1.5038634
[8] T. Hirai et al., “Use of tungsten material for the ITER divertor”, Nuclear Materials and Energy 9 (2016) 616-622. https://doi.org/10.1016/j.nme.2016.07.003
[9] M.H. Aumeunier et al., “Infrared Thermography in Metallic Environments of WEST and ASDEX Upgrade”, Nuclear Materials and Energy 26 (2021) 100879. https://doi.org/10.1016/j.nme.2020.100879
[10] J. Gaspar et al., “Emissivity measurement of tungsten plasma facing components of the WEST tokamak”, Fusion Engineering and Design 149 (2019) 111328. https://doi.org/10.1016/j.fusengdes.2019.111328
[11] J. Gaspar et al., “Overview of the emissivity measurements performed in WEST: in-situ and post-mortem observations”, Nuclear Fusion, accepted paper. https://doi.org/10.1088/1741-4326/ac6f68
[12] M. Firdaouss et al., “First feedback during series fabrication of ITER like divertor tungsten components for the WEST tokamak”, Physica Scripta 96 (2021) 124037. https://doi.org/10.1088/1402-4896/ac2978
[13] J. Bucalossi et al., “Operating a full tungsten actively cooled tokamak: overview of WEST first phase of operation”, Nuclear Fusion 62 (2022) 042007. https://doi.org/10.1088/1741-4326/ac2525
[14] M. Missirlian et al., “The WEST project: Current status of the ITER-like tungsten divertor”, Fusion Engineering and Design 89 (2014) 1048-53. https://doi.org/10.1016/j.fusengdes.2014.01.050
[15] M. Richou et al., “Acceptance tests of the industrial series manufacturing of WEST ITER-like tungsten actively cooled divertor”, Physica Scripta 96 (2021) 124029. https://doi.org/10.1088/1402-4896/ac2657
[16] N. Chanet et al., “Design and integration of femtosecond Fiber Bragg gratings temperature probes inside actively cooled ITER-like plasma-facing components”, Fusion Engineering and Design Volume 166, May 2021, 112376. https://doi.org/10.1016/j.fusengdes.2021.112376
[17] R.A. Pitts et al., “Physics conclusions in support of ITER W divertor monoblock shaping”, Nuclear Materials and Energy 12 (2017) 60-74. https://doi.org/10.1016/j.nme.2017.03.005
[18] A. Grosjean et al., “Interpretation of temperature distribution observed on W-ITER-like PFUs in WEST monitored with a very-high-resolution IR system”, Fusion Engineering and Design 168 (2021) 112387. https://doi.org/10.1016/j.fusengdes.2021.112387
[19] J. Gaspar et al., “In-situ assessment of the emissivity of tungsten plasma facing components of the WEST tokamak”, Nuclear Materials and Energy, 25 (2020) 100851. https://doi.org/10.1016/j.nme.2020.100851
[20] M. Houry et al., “The very high spatial resolution infrared thermography on ITER-like tungsten monoblocks in WEST Tokamak”, Fusion Engineering and Design 146 (2019) 1104–1107. https://doi.org/10.1016/j.fusengdes.2019.02.017

[21] E. Gauthier et al., “Confocal microscopy: A new tool for erosion measurements on large scale plasma facing components in tokamaks”, Journal of Nuclear Materials 538 (2013) S1216–1220. https://doi.org/10.1016/j.jnucmat.2013.01.269
[22] F. Gallay et al., “Quantitative thermal imperfection definition using non-destructive infrared thermography on an advanced DEMO divertor concept”, Phyica Scripta 2017 014015. https://doi.org/10.1088/1402-4896/aa878e
[23] H. Greuner et al., “High heat flux facility GLADIS: operational characteristics and results of W7-X pre-series target tests”, Journal of Nuclear Mateials 367–370 1444–8. https://doi.org/10.1016/j.jnucmat.2007.04.004
[24] H. Greuner et al., “Results of high heat flux qualification tests of W monoblock components for WEST”, Physica Scripta 2017 T170. https://doi.org/10.1088/0031-8949/2017/T170/014001
[25] Y. Corre et al., “Sustained W-melting experiments on actively cooled ITER-like plasma facing unit in WEST”, Physica Scripta 96 (2021) 124057. https://doi.org/10.1088/1402-4896/ac326a
[26] M. Balden et al., “Erosion and redeposition patterns on entire erosion marker tiles after exposure in the first operation phase of WEST”, Physica Scripta 96 (2021) 124020. https://doi.org/10.1088/1402-4896/ac2182
[27] J. Gaspar et al. “Divertor power loads and scrape off layer width in the large aspect ratio full tungsten tokamak WEST”, Nuclear Fusion 61 (2021) 096027. https://doi.org/10.1088/1741-4326/ac1803